Food Chemistry 233 (2017) 457–466

Contents lists available at ScienceDirect

Food Chemistry

journal homepage: www.elsevier.com/locate/foodchem

A saliva molecular imprinted localized surface plasmon resonance biosensor for wine astringency estimation

J. Rafaela L. Guerreiro [c,a,b], Natércia Teixeira [b], Victor De Freitas [b], M. Goreti F. Sales [a], Duncan S. Sutherland [c,*]

[a] BioMark Sensor Research-CINTESIS, Instituto Superior de Engenharia do Porto, Porto, Portugal
[b] QUINOA-LAQV-REQUIMTE, Departamento de Química e Bioquímica, Faculdade de Ciências da Universidade do Porto, Porto, Portugal
[c] Interdisciplinary Nanoscience Center (iNANO), Aarhus University, Aarhus, Denmark

ARTICLE INFO

Article history:
Received 28 July 2016
Received in revised form 10 April 2017
Accepted 10 April 2017
Available online 12 April 2017

Keywords:
PCA
Polyphenols
Wine
Astringency
Molecular imprinted polymers
LSPR

ABSTRACT

Wine astringency was evaluated based on the interaction of two complex matrices (red wine and saliva) by combining localized surface plasmon resonance (LSPR) and molecular imprinted polymers (MIP) at gold nanodisks as an alternative to sensorial analysis. The main objective of the work was to simulate wine astringency inside the mouth by mimicking this biological system. The LSPR/MIP sensor provided a linear response for astringency expressed in pentagalloyl glucose (PGG) units in concentrations ranging from 1 to 140 μmol/L. The sensor was also applied to wine samples correlating well with sensorial analysis obtained by a trained panel. The correlation of astringency and wine composition was also evaluated showing that anthocyanins may have an important role, not only for pigmentation but also in astringency.

1. Introduction

Polyphenols are among the most abundant compounds in the human diet. Colour, smell and taste, amongst other sensorial characteristics of food products, result directly from the presence of polyphenols or from their collective action such as astringency. Astringency is generally accepted to result from the interaction between polyphenols present in food matrixes and salivary mouth proteins, decreasing mouth lubrication and leading to dryness, puckering and constriction of the tissues. The interactions between polyphenol and protein are characterized by the formation of complexes that might extend to larger complexes and finally lead to precipitation. However, the initial complexation between polyphenols and proteins seems more closely associated to astringency than the later precipitation (Obreque-Slier, Lopez-Solis, Pena-Neira, & Zamora-Marin, 2010).

Astringency is a sensorial parameter that is especially important for wine production, determining the product quality, and for that reason requires an accurate control. Wine polyphenols comprise an enormous family of compounds such as anthocyanins, condensed tannins extracted from grapes and stable/more complex derived compounds that generally result from oxidation, degradation and even precipitation (between condensed tannins/anthocyanins) during wine aging (He et al., 2012). Not all polyphenols in wines come from the grapes; some compounds like hydrolysable tannins (e.g. pentagalloyl glucose) might be added during wine production or result from their migration along the contact between wine and oak barrels (Sarneckis et al., 2006). Astringency of wine polyphenols has also been associated with their individual characteristics, such as concentration, polymerization degree, molecular weight and number of galloyl substituents of polyphenols (Batesmit, 1973; Hagerman & Robbins, 1987; Kawamoto, Nakatsubo, & Murakami, 1995).

Wine is a complex matrix due to the variety of polyphenols directly extracted from grapes, as well as due to their ability to undergo numerous interactions and chemical reactions changing the overall polyphenol profile over time. Wine astringency evaluation is therefore a tough task and even with the use of sensorial analysis the results are subjective, time-consuming and expensive (Vidal et al., 2004). Regardless of the disadvantages, sensorial panels with several elements remain the most common approach to evaluate astringency. These sensorial panels are normally composed of professionals that can also be trained with several standard solutions prior to wine astringency evaluation. Despite that,

* Corresponding author.
E-mail address: duncan@inano.au.dk (D.S. Sutherland).

http://dx.doi.org/10.1016/j.foodchem.2017.04.051
0308-8146/

salivary protein production also varies with the time of the day, food consumption, diet, circadian rhythms, age, gender, several disease states and pharmacological agents (Dodds, Johnson, & Yeh, 2005). Therefore, the development of more effective methods to assess astringency and understand the mechanisms of action between polyphenols and proteins is of great importance.

Different methods have been applied to study astringency at the molecular level based on precipitation studies between specific proteins (gelatin, BSA, mucins,...) or salivary proteins and individual or mixture of polyphenols, thus evaluating the protein fraction before and after precipitation. The direct and/or indirect quantification of polyphenols has also been used as an alternative way to estimate astringency (Caceres-Mella et al., 2013; Guerreiro, Sutherland, De Freitas, & Sales, 2013). However, astringency does not always correlate well with precipitation assay or polyphenol content.

Other techniques such as SDS-PAGE (Rinaldi, Gambuti, & Moio, 2012), spectrophotometry (Simoes Costa, Costa Sobral, Delgadillo, Cerdeira, & Rudnitskaya, 2015), fluorescence (Fia, Dinnella, Bertuccioli, & Monteleone, 2009), nephelometry (Monteleone, Condelli, Dinnella, & Bertuccioli, 2004), NMR (Furlan, Jobin, Pianet, Dufburc, & Gean, 2015), DLS (Pascal, Poncet-Legrand, Cabane, & Vernhet, 2008) and mass spectrometry (Careri, Corradini, Elviri, Nicoletti, & Zagnoni, 2004) have also been used to study proteins and polyphenols interactions with and without the focus on astringency. Generally, the methods used to assess astringency also compare the new methods with sensorial analysis performed by a trained panel. The emergence of new technologies allowed the study of these interactions, not just at the molecular level, but likewise at the nanoscale through nanotechnology such as localized surface plasmon resonance (LSPR) (Guerreiro et al., 2014).

Considering the complexity of astringency mechanisms and variation in astringency estimation by different approaches, these effects suggest that for each class of polyphenol the astringency phenomenon may be different, while the synergetic effects play an important role. Therefore, the methods that consider the global mechanism at the molecular/atomic level seem to be the most suitable for astringency estimation in beverages.

Recently, LSPR sensors were reported for the detection and quantification of biomolecules, via specific interactions due to their high sensitivity, good reproducibility, real-time responses and potential for label-free detection. LSPR's are collective oscillations of conduction electrons at confined metal nanostructures formed from metals such as Au, Ag, Al and are typically probed by interaction with light. The highly sensitive dependence of the resonance energy on the refractive index (RI) surrounding the metal nanostructure means that biomolecules adsorption on the metal surroundings causes the shift of the LSPR peak wavelength, with larger RI changes giving large shifts. Generally, antibodies are used as biomolecular recognition elements immobilized at the surface of a sensor. Nevertheless, new artificial antibodies also known as molecular imprinted polymers (MIPs) have been developed to improve the stability of sensory devices. The design of molecular imprinted materials involves the copolymerization of monomers and cross-linker elements in the presence of the target molecule. After polymerization the target molecule is removed by an appropriate method from the polymeric matrix, leaving imprinting sites with complementary shape, size and functional chemistry to the target molecule, which leads to selectivity on rebinding. The integration of MIPs technology with plasmonic sensors results in a combination of a high sensitivity biosensor method coupled with robustness, stability and reusability features.

The main purpose of this work was to develop a sensor device combining LSPR and MIPs to evaluate wine astringency at the molecular/atomic level, compare sensorial and analytical wine astringency and then correlate astringency with wine composition. We used salivary proteins as target molecules and aqueous compatible monomers cross-linked in a polymer network with specific binding sites at gold nanodisks for salivary proteins through a surface imprinting process. The interactions between polyphenol and protein used salivary proteins and pentagalloyl glucose (PGG) for sensor calibration, followed by real wine samples analysis and astringency estimation.

2. Experimental

2.1. Apparatus

QCM-D measurements were performed with the Q-sense E4 system (Q-sense AB) using the 7th, 9th and 11th overtones recording both frequency and dissipation. AT-cut quartz crystals with a fundamental frequency of 5 MHz were purchased from Q-sense AB (Sweden) with gold electrodes.

SPR measurements were performed with a Biacore X system from Biacore AB (Sweden) and gold SPR chips were purchased from GE Healthcare.

Prior to any measurement, both QCM crystals and SPR chips were cleaned by basic piranha solution consisting of MilliQ water (MQ), ammonia 25% and hydrogen peroxide 30% (5:1:1) at 75 °C for 5 min, followed by rinsing with MQ and blow dried with nitrogen. In order to finalize the cleaning procedure, the substrates were treated with 10 min of UV/ozone (Kern & Puotinen, 1970).

LSPR measurements were performed in a Shimadzu UV–Vis–NIR spectrophotometer UV-360 using a flow injection cell and wavelength ranging from 400 to 900 nm. Extinction spectra were collected in the absorbance mode.

Wine characterization assays were performed in an UV–vis spectrophotometer Thermo Scientific Evolution Array UV–vis spectrophotometer, a HACH 2100 N turbidimeter equipped with a 100 × 12 mm cell adaptor, and a Thermo® Scientific HPLC with a Thermo® Scientific Spectra System P4000 pump on a 250 × 4.6 mm i.d. reversed-phase C18 column (Merck®, Darmstadt) at 25 °C; detection was carried out between 200 and 800 nm using a Thermo® Scientific Spectra System UV8000 diode array detector; 20 µl of each sample was injected using an autosampler Thermo® Scientific Spectra System AS3000.

2.2. Reagents and solutions

All chemicals were of analytical grade. Buffers were prepared with MQ, additional filtering (0.2 µm pore filter) and sonication was required for both QCM-D and SPR experiments. The used buffers were: 10 mM PBS (Phosphate buffered saline) pH 7, PBS with 5% Ethanol and 50 mM ammonium bicarbonate (AMBIC) supplied by Sigma-Aldrich. PGG standard solutions were prepared in PBS 5% ethanol.

The fabrication of gold nanodisks involved the use of polymethylmethacrylate Mw 495,000, 4% anisole (PMMA) purchased from Micro resist technology GmbH, poly(diallyldimethylammonium chloride) (PDDA), poly(sodium-4-styrenesulfonate) (PSS) purchased from Sigma-Aldrich, polyammonium chloride (PAX) purchased from KemiraMiljø and polystyrene (PS) colloidal particles acquired from Invitrogen.

Gold (flat or nanodisks) surface modification included 16-mercaptohexadecanoic acid, 99% from Assemblon, *N*-Hydroxysuccinimide (NHS) and 1-Ethyl-3-(3-dimethylaminopropyl) carbodiimide (EDAC) purchased from Aldrich.

The imprinted process required thiophenecarboxylic acid (TPCA), methacrylic acid (MAA), (vinylbenzyl)trimethylammonium

chloride 97% (VTMA), ethylene glycol dimethacrylate 98% (EGDMA), ammonium persulfate (AP), methyl acrylate 99% (MA) from Sigma-Aldrich.

Bovine serum albumin (BSA) was also obtained from Sigma-Aldrich.

2.3. Saliva collection

Saliva was collected from 20 healthy non-smoking volunteers; with ages between 20 and 42 years old for 2 h prior any food consumption (only drinking water was allowed). Saliva collection took around 60 min. Immediately after collection, all the saliva samples were mixed together, filtered with a syringe filter of 0.2 μm size and frozen at −20 °C, in aliquots of 100 μL. Values for dn/dc for the saliva was carried out using a differential refractometer at standard conditions (BI-DNDC differential refractometer λ = 620 nm t = 30 °C). The saliva was desalted using 4 sequential rounds of spin concentration (∼10 times up concentration) using 3 kD cut off filters and dilution in deionised water. Some aliquots were then dried at 120 °C for 30 min and weighed to obtain the concentration and others were diluted to the experimental buffer conditions at a series of concentrations and dn/dc determined.

2.4. Au nanodisks fabrication

Glass slides from menzel-glass were first cleaned by acetone wiping and O_2 plasma cleaning for 15 min (RF 100 watt, pressure 25 mtorr) followed by PMMA spin coating (3000 rpm, 1000 rpm/sec^2 for 1 min) and 180 °C baking for 2 min to obtain a 200 nm thick layer. The nanostructures were then prepared by sparse colloidal lithography. This methodology consisted on a triple layer of polyelectrolytes – 2% PDDA, 2% PSS and 5% PAX in MQ – each solution was added to the surface for 30 s followed by MQ rinsing for 1 min and then self-assembly of charged polystyrene particles diameter 100 nm (Invitrogen, 0.2% in MQ) for 2 min and 90 s MQ rinsing. The substrates were carefully dried under a stream of nitrogen gas and treated with 90 s of UV/ozone. Substrates were then coated with 20 nm Ti by electron beam-stimulated thermal evaporation physical vapor deposition (EB-PVD, Cryofox, Polyteknik AS, DK) at a deposition rate of 0.2 Å/s and ion beam assisted for the first 15 s of the evaporation (anode current 0.3 A, anode voltage 100 V and neutral current 150 mA). Tape was used to remove the PS particles and by etching (RF 50 watt, 40 sccm oxygen flow and pressure 25 mtorr, Vision 300 MK II, Advanced Vacuum AB, Sweden) the PMMA underneath the revealed holes in the titanium film was also removed. A second evaporation at 1 Å/s, deposited 2 nm Ti as adhesion layer followed by 20 nm Au. The Ti sacrificial mask was then removed by acetone rinsing leaving on the glass surface the Ti/Au disks (2/20 nm, diameter 100 nm). Prior to biosensing experiments, the samples were exposed to ethanol and MQ for 2 min each in the sonicator followed by UV/Ozone for 30 min. The samples were then in MQ water for at least 1 h to reduce the gold to Au^0. The procedure for Au nanodisks fabrication is illustrated in supplementary information, figure S1.

2.5. Imprinting procedure

The gold substrates (QCM-D and SPR chip surface or disks nanostructures) were functionalized using 2 mM 16-mercaptohexadecanoic acid in ethanol overnight. The samples were then rinsed with ethanol and MQ for 3 min each in a sonicator to remove any unbound thiols and dried with a stream of nitrogen. To amine couple salivary proteins, the carboxyl terminated thiol was activated through the addition of 400 mM EDAC/200 mM NHS followed by MQ rinsing to remove un-reacted species. The substrates were then incubated in saliva to allow the covalent attachment of proteins present in saliva and the gold substrates.

Before polymerization different charged monomers were added to the modified surface for 30 min each in the following order: 5 mM VTAC in MQ, 2 mM TPCA in 10% ethanol and 5 mM MAA in MQ, between incubations the substrates were rinsed with MQ.

Polymerization was then initiated by adding the polymerization mixture containing EDGMA, MA and AP 5 mM to the surface at 39 °C over-night. After polymerization, the surface was thoroughly rinsed with MQ and the attached salivary proteins removed by enzymatic cleavage through proteinase k 500 μg/mL at 37 °C. To wash away the peptide fragments, PBS pH 7.4, AMBIC pH 8 and MQ were rinsed through the surface, followed by N_2 drying.

In parallel, non-imprinted polymer (NIP) materials which excluded the surface functionalization with carboxyl thiol, activation of functional group and saliva coupling were prepared as controls.

2.6. Imprinting procedure by QCM-D, SPR and LSPR measurements

Both QCM-D and SPR were performed on homogeneous gold samples.

For QCM, during rinsing and exchange of buffers, liquid was pumped over the sensors with a flow rate of 0.1 mL/min. For SPR, the flow rate was set to 10 μL/min and injection volumes were 100 μL giving a maximum injection time of 10 min. The temperature was 23 °C and 37 °C, before and after polymerization, respectively.

QCM experiments: First, the substrates were modified with 2 mM 16-mercaptohexadecanoic acid in ethanol overnight outside the flow system. After achieving a stable baseline in PBS, both activation agents (NHS/EDAC) were introduced and allowed to react for 10 min in stop flow. Secondly, after rinsing for 20 min with PBS, saliva was allowed to interact with the surface by pumping through the sensor surface 400 μL of saliva with a flow rate of 0.1 mL/min. The pump was, thereafter, stopped and the proteins allowed to interact under static conditions for 1 h. The surfaces were finally rinsed with PBS buffer until achieving stable measurements.

Polymerization was carried out outside the flow system in the same conditions as described before. After polymerization, a new stable baseline was achieved in PBS at 37 °C with a flow rate of 0.05 mL/min. The removal of salivary proteins from binding sites was achieved by pumping to the surfaces 500 μL of proteinase k, stopping the flow for 2 h and rinsing the sensors with PBS buffer.

SPR experiments: These were performed in similar conditions as QCM-D except incubation time of saliva and proteinase k which were 10 min each and the activation by NHS/EDAC was performed in continuous flow instead of batch mode.

LSPR experiments: These were performed in similar conditions as QCM-D and SPR. Activation by NHS/EDAC was performed for 10 min, saliva incubated for 30 min and proteinase k for 2 h at 37 °C, all in batch conditions.

2.7. LSPR interaction measurements

The imprinted materials were placed in a home-made flow cell (Figure S2, supplementary data). The cell consisted of a chamber created by two glass sides held in place by a vacuum system with the flow passing between the two glass substrates. The measurements were performed in a double beam system, with a reference (two glass slides) and a sample (glass slide/Au nanodisks glass slide). The flow-rate was controlled by a peristaltic pump and set to 55 μL/min.

The measurements started by collecting the LSPR extinction spectra in PBS buffer as a baseline. Before exchanging each solu-

tion, a spectrum was collected to obtain the LSPR peak position. After baseline collection, saliva rebinding was achieved by injecting saliva for ~20 min in continuous flow followed by 5 min of PBS buffer. The buffer was then exchanged for PBS buffer with 5% ethanol, in order to verify the effect of the buffer on the refractive index change. Subsequently, increasing concentrations of PGG solutions were injected in the chamber for 150 s followed by PBS 5% ethanol to wash weakly attached PGG molecules. The surface rinsing with BPS 5% ethanol for 150 min would simulate the behaviour inside the mouth by increasing the pH values to neutral without ignoring the wine effect after consumption (Brand, Fat, & Veerman, 2009). Spectra were collected from 500 to 900 nm after 150 s in PBS 5% ethanol to assure a stable response. PGG concentrations ranged from 1.0 to 140 μM. The plotted calibration curves reproduced peak shift *versus* log cumulative PGG concentrations.

The measurements were carried out using the imprinted and non-imprinted materials. Additionally, the rebinding to imprinted materials without saliva also acted as a control.

2.8. Wine characterization

Wine samples were provided by the Portuguese organization CVRVV, abbreviation for "Comissão de Viticultura da Região dos Vinhos Verdes", which has kindly characterized all the wine samples by sensorial analysis. Sensorial analysis was performed by a tasting panel of three tasting specialists and one panel leader. Samples were presented to the panel blind and coded. Each tasting expert performed the sensorial analysis and filled in a sensory sheets with sensory attributes namely appearance, odour and flavour. The overall verdict is made by all the elements and based on their tasting records. Sensorial analysis was performed in a proper and ventilated room at 20 ± 2 °C, under natural light. Wine astringency was classified on a scale of 1–10 with 10 being the most astringent and 1 the less astringent wine.

These samples were chemically characterized in terms of: total phenolic content (TPC) determined by UV absorbance at 280 nm of the absorbance capacity of phenolic rings (Somers & Ziemelis, 1985) (1 mm optical path cell); total proanthocyanic tannins determined by Bate-Smith reaction which consisted on the acid hydrolysis of condensed tannins, at 100 °C for 30 min, to form the respective anthocyanins (Ribéreau-Gayon & Stonestreet, 1966); tannin power to determine the polyphenols capacity to precipitate bovine serum albumin (BSA) measured by nephelometry (Freitas, 1995); dialysis index to determine the complexity degree of polyphenols (Glories, 1978; Mateus, Proenca, Ribeiro, Machado, & Freitas, 2001); free anthocyanins determined by adaptation of the bisulphite method (Somers & Evans, 1977) and monoglucosidic anthocyanins determined by HPLC (Roggero, Larice, Rocheville-Divorne, Archier, & Coen, 1988).

The colour characteristics, were evaluated by the red colour index (RCI) at A520 nm, colour index (CI) A420 + A520 + A620 nm, measuring directly absorption at 420, 520 and 620 nm (1 mm optical path), and CIELab colour coordinates (L^*, C^*, H^*), where L^* is the lightness, C^* the chromaticity and H^* hue, measured by direct absorption (2 mm optical path) and determined by ColorWin-MSCV® Coordinates software.

LSPR sensor was used to evaluate the astringency of wine samples, expressed in PGG. Astringency determination was performed similarly to the LSPR interaction measurements, but instead of interacting saliva with PGG, the interaction was made directly with real wine samples diluted 20-fold. Saliva was injected for ~20 min in continuous flow for rebinding, thus followed by 90 s in PBS buffer. Sensor devices regeneration was carried out by incubating the surface in 100 μL proteinase k over-night at 37 °C.

2.9. Statistical treatment

The statistical data analysis was performed by the principal component analysis (PCA) with the Addinsoft XLSTAT software, using standardized values as input, calculated as ($Value_{parameter}$ − $Average_{parameter}$)/$Standard\ deviation_{parameter}$).

PCA was applied to a data set of 13 attributes (total phenolic content, proanthocyanic tannins, tannin power, dialysis index, free anthocyanins, monoglucosidic anthocyanins, colour coordinates, red colour index, colour index, sensorial astringency and analytical astringency). Data on the different attributes was used to characterize the 9 wine samples. PCA analysis explains the differences between wines by means of different attributes indicating which variable contribute most for the obtained differences.

2.10. β-1,2,3,4,6-Penta-O-galloyl-d-glucopyranose (PGG) synthesis

PGG was synthesized from tannic acid according to the method of Chen and Hagerman (Chen & Hagerman, 2004). Briefly, 5.0 g of tannic acid was dissolved in 70% methanol in acetate buffer (0.1 M, pH 5.0) at 65 °C for 15 h. After this time, the pH of the mixture was immediately adjusted to 6.0 with NaOH. Methanol was then removed by evaporation under reduced pressure at <30 °C and extracted with 3 volumes of diethyl ether and 3 volumes of ethyl acetate. The ethyl acetate extracts were combined and evaporated. The resulting suspension was centrifuged, and the precipitate was redissolved by heating in 2% methanol solution. PGG precipitated as the solution cooled to room temperature and was collected by centrifugation. PGG was washed twice with an ice-cold 2% methanol solution and once with ice-cold distilled water. The final material was lyophilized to yield a white powder with an overall mass yield of 23%. The purity of the obtained PGG was assessed by HPLC analysis and 1H NMR spectroscopy. PGG was generously provided by the Chemistry and Biochemistry Department of Faculty of Sciences of Porto University.

3. Results and discussion

3.1. Molecular imprinted materials

Astringency measures the interaction between proteins and polyphenols in wines, meaning that an astringency sensor should have saliva proteins as biorecognition element. But an astringency sensor should also hold a stable sensing layer, in order to have a wide lifespan and little storage requirements. In addition, there are different proteins on saliva interacting with polyphenols, and therefore the sensing layer should also reflect such complex composition. Thus, the development of a biomimetic surface that could allow reproducing a saliva surface on-site would be of interest.

In this regard, molecularly-imprinted materials are well-known by their ability to generate biomimetic surfaces, offering good stability and ability to recognize the imprinted target molecule (Whitcombe et al., 2011). So, surface imprinting was established on a gold support having as template the complex saliva matrix. Rebinding was established when needed with the saliva sample, followed by interaction with wine polyphenols. The response of the sensor was checked specifically against PGG and expressed in PGG equivalents (calibrated by the interaction between salivary proteins and PGG).

The first stage of the imprinting process consisted of attaching the proteins from saliva to the gold surface. This was made by nucleophilic substitution on the carboxyl terminated functional group of the thiol compound with the primary amine groups in the proteins. For this purpose, the gold surface was first modified with a carboxyl terminated thiols over-night, allowing the gold/

thiol bonding and the ordered packing of the long fatty acid chains and Van der Vaals interaction. The coupling agents (NHS/EDAC) were added to the surface, activating the thiol carboxyl groups through the carbodiimide chemistry, leading to the formation of amine reactive NHS esters. These esters are very reactive with primary amines on the exposed surface of proteins, forming stable amide bonds that result in protein covalent attachment to the surface.

The imprinted material is obtained next by growing a polymeric structure around the adsorbed proteins and removing the proteins from the so formed polymeric moulds. Such moulds should correspond to specific recognition sites on the polymeric matrix, with the combination of complementary shape, size, orientation and chemical affinity to the target molecule. Surface imprinting was the approach taken herein, to increase the number of rebinding sites formed and facilitate protein removal. The stability of the imprinted polymer was enhanced by adding TPCA to the surface with proteins (before polymerization), ensuring that the polymer formed next would bind covalently to the transducer support. The affinity between each protein and its binding site was enhanced by adding two opposite charged monomers (VTAC, MAA) to the substrate holding the protein covalently attached, these charged monomers established strong electrostatic and Van der Vaal's interactions with the proteins, while participating in the polymerization stage, thereby promoting complementary mould with charged positions (protein recognition is expected to rely on its shape and also on its complementary charged positions). The polymerization took place on the previous surface containing a mixture of neutral monomer (MA), cross-linker (EDGMA) and initiator (AP). Such polymeric material is expected to create two distinct chemistries: the areas around the proteins and the overall material. The recognition sites (areas with imprinted proteins) are the ones where the charged monomers remained, providing the region with the chemical complementarity of proteins. Moreover, the other locations on the polymer surface are neutral in terms of charge, avoiding competition with binding sites and subsequently leading to an increased selectivity of the polymer to recognize the imprinted proteins.

After polymerization, the proteins embedded on the polymer were removed by enzymatic digestion. Proteinase k was added for 2 h at the optimal temperature of 37 °C to digest the proteins at the binding sites. The broad cleavage specificity of proteinase k resulted in several protein fragments which were then washed away by thorough rinsing with AMBIC and MQ. Simultaneously, non-imprinted materials were also produced exactly in the same way with exception of the protein covalent attachment step, to act as experiment controls.

The imprinted polymer materials resulted in complex sensing surfaces based on the large variety of proteins in saliva which were then characterized by QCM-D, SPR and LSPR before the wine samples analysis.

3.2. Characterization of saliva layer by QCM-D and SPR measurements

Molecular imprinted polymers specific for salivary proteins were characterized by the combination of QCM-D and SPR experiments.

The QCM-D experiments were performed on a flat gold chip measuring frequency and dissipation shifts over time. Prior to the start of the measurements the gold surfaces were chemically modified with carboxyl terminated thiol. The surfaces were then placed in the QCM-D chamber with a constant flow in order to initiate the covalent immobilization of proteins from saliva. Fig. 1A shows the saliva immobilization step which consisted of: a) the activation of the carboxyl terminated thiol by NHS/EDAC injection and; b) covalent binding of salivary proteins. The imprinting step was performed outside the chamber over-night at 39 °C. The substrate was then replaced in the chamber until reaching a stable baseline at 37 °C and c*) exposed to proteinase k for 2 h with stop flow.

Surface activation slightly decreases frequency and increases dissipation, whereas the salivary proteins induce a large and irreversible protein attachment of ~50 Hz reducing the frequency and increasing dissipation. After the imprinting step, QCM-D measurements were also performed to evaluate the protein removal step. Proteinase k induces an increase in frequency of ~25 Hz and a decrease in dissipation, indicating that only salivary proteins are being removed from the polymer material.

According to Fig. 1B, the comparison dissipation *versus* frequency shows the relationship between mass adsorbed per unit mass on gold with changes in rigidity. During protein attachment we can see a linear behaviour in the beginning of the process which becomes slightly curved until the end, indicating possible conformational changes of the protein layer or change in the hydration state. During protein removal the $\Delta D/\Delta F$ value is linear and significantly constant when compared to the attachment step supporting the idea that the kinetics for protein removal is slower and does not involve conformational changes.

Considering the high values of dissipation obtained herein and that proteins form non-rigid layers, the accurate quantitative analysis using dissipation and frequency values should be calculated by the Voigt viscoelastic model. The model was applied to analyze the measured changes in frequency, Δf, and dissipation, ΔD, for constant values of bulk fluid density, bulk fluid viscosity and protein layer density in order to extract information on layer thickness (m), shear elasticity (Pa) and viscosity (kg/ms). The thickness and density parameters are not independent variables, therefore the model generates pares of thickness and density values (Q-tools software 2.0.6, Q-sense AB). These two parameters allow the calculation of the total Voigt mass of the film (layer density times effective thickness), which includes both protein and water mass. However, to calculate the effective film thickness, the layer density needs to be independently known. In order to calculate the effective density of the protein layer, additional information on the protein mass is required and it can be obtained by an independent measurement as SPR. The SPR mass can be calculated based on the change in the resonance angle via Eq. (1)

$$m_{spr} = d\frac{dc}{dn}k\frac{\Delta\theta}{1-e^{-2d/l_{decay}}} \quad (1)$$

where d (m) is the effective thickness of the film obtained from QCM-D modelling, dc/dn (kg/m^3) is the inverse refractive index increment for the adsorbed molecule, k (deg^{-1}) is the sensitivity factor of the system, $\Delta\theta$ (deg) is the change in resonance angle and l_{decay} (m) is the decay length of the evanescent field. The values for k and l_{decay} where assumed according to the values obtained by Malmström et al. (Malmstrom, Agheli, Kingshott, & Sutherland, 2007) whereas dn/dc was calculated using the experimentally determined value of 0.173 mL/g.

SPR measurements, Fig. 2, allowed the dry mass quantification of protein layer covalently immobilized (without considering water molecules) which was then used to calculate the effective density.

The QCM-D modelling provided the effective thickness of the protein layer for a given density. The dry protein density was set to 1330 kg/m^3 (Hook et al., 2002), and the initial guess for the layer density, generating a result for the effective thickness and layer density used to calculate the total Voigt mass. The combination of Voigt mass and SPR mass through Eq. (2) allowed the calculation of the effective density of protein layer.

$$\rho_{layer} = \frac{m_{Voigt}}{\frac{m_{SPR}}{\rho_{protein}} + \frac{m_{Voigt}-m_{SPR}}{\rho_{water}}} \quad (2)$$

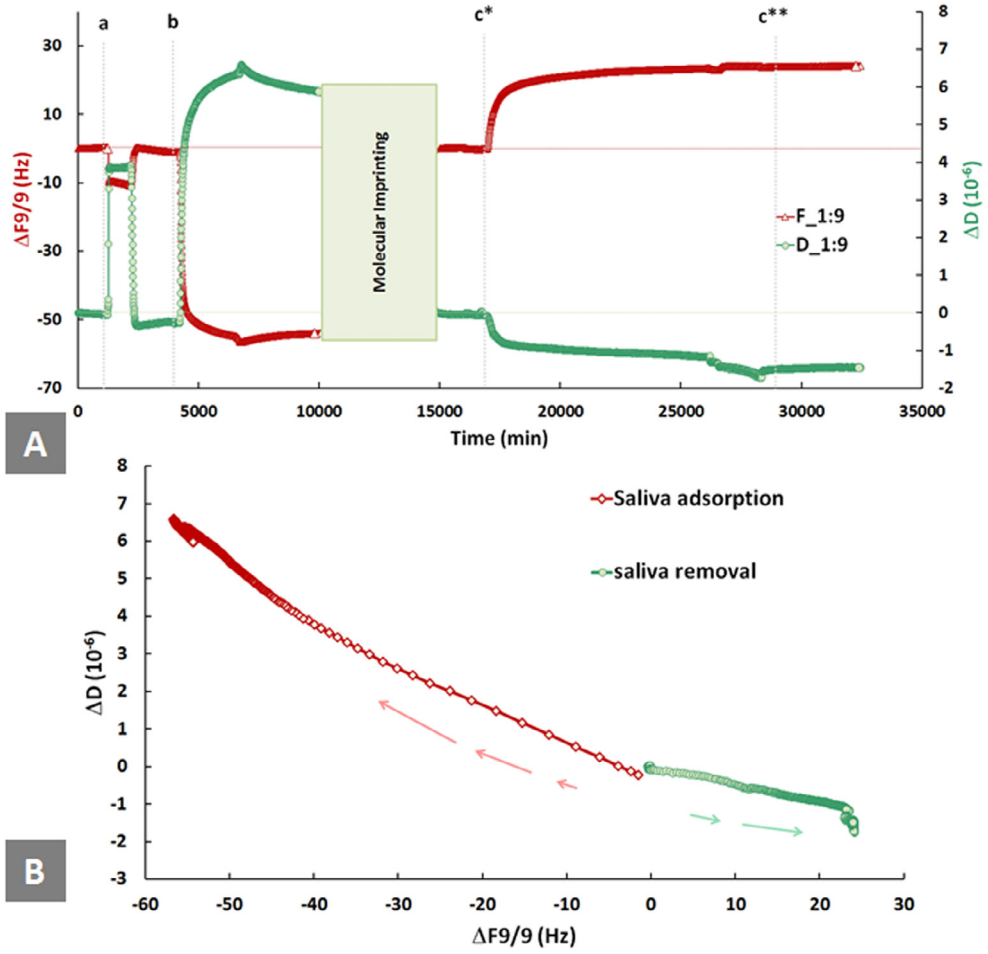

Fig. 1. QCM-D measurements (A) showing the change in frequency and dissipation shifts during the imprinted process on the Au nanodisk (a) activation of the Au surface (b) saliva adsorption (c*) introduction of proteinase k in the system at 37 °C and stop of the flow rate (c**) restart of flow rate for saliva removal. (B) QCM-D data plotted as change in dissipation *versus* change in frequency for saliva adsorption and removal. The arrows indicate the experimental flow.

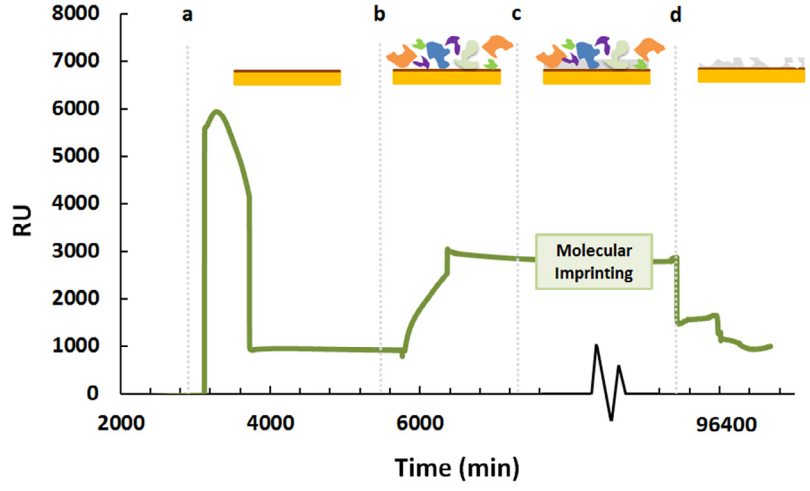

Fig. 2. SPR experiments of the molecular imprinting process. (a) Activation of the Au surface (b) saliva adsorption (c) polymerization of molecular imprinted material (d) saliva removal by proteinase k at 37 °C.

The effective layer density obtained by Eq. (2) was then used in QCM-D modelling to obtain a new layer thickness and density in a continuous iterative process until convergence was reached. The mass and thickness obtained by QCM-D and SPR for the salivary protein layer are summarized in Table 1.

The covalent attachment of salivary proteins on a gold surface showed a thickness of ~14 nm, which is reasonable for a monolayer of mixed proteins (Warkentin, Walivaara, Lundstrom, & Tengvall, 1994). The layer indicated high hydration with ~89% water, following the trend that larger proteins result in more

Table 1
Summary of results obtained from QCM-D and SPR measurements for saliva immobilized on Au surface.

Viscoelastic model		
Layer properties	Saliva adsorption	
$m_{QCM\ (WET)}$, ng/cm^2	1476 ± 176	
$m_{SPR\ (DRY)}$, ng/cm^2	167.6 ± 0.9	
Calculated Thickness, nm	14.3 ± 1.8	
Calculated Density, kg/m^3	1029.3 ± 3.3	
Layer Hydration level	89%	
Raw data		
Layer properties	Saliva adsorption	Saliva removal
RUspr	1885 ± 31	−1454 ± 313
SPR, ng/cm^2	154.6 ± 2.5	−119.3 ± 25.7
Δf QCM, Hz	−52.7 ± 2.8	24.5 ± 0.7
ΔD QCM($\times 10^{-6}$)	6.15 ± 0.1	−2.0 ± 0.8

hydrated protein layers. The salivary protein layer (which contains a mixture of proteins including many glycosylated proteins (Guerreiro et al., 2016)) showed a density of 1029.3 ± 3.3 kg/m^3, which corresponded to the mass ratio of water to protein of 8 (Malmstrom et al., 2007). The combination of QCM-D and SPR has allowed quantifying the properties of the salivary proteins layer formed when covalently attached to a gold surface. Additionally, salivary proteins removal was also followed as can be seen by the raw QCM-D and SPR data, indicating that most proteins were not trapped on the molecular imprinting polymer which is essential to further protein recognition during rebinding events. Modelling of the QCM-D data during protein removal did not fit the experimental data probably due to the non-continuous nature of any remaining protein.

3.3. LSPR combined with MIP sensor

To understand the interaction within salivary proteins and pentagalloyl glucose (PGG) molecular imprinting, stabilized polymers were combined with Au nanodisks arrays. First, Au nanodisks (diameter 100 nm and 20 nm height) were fabricated on glass substrates through hole mask colloidal lithography (Fredriksson et al., 2007). Briefly, PMMA polymer is spin coated on the clean glass samples to give a 200 nm thick layer followed by polyelectrolytes assembly. Basic electrostatic self-assembly to adsorb the charged polystyrene particles 100 nm (PS) onto the oppositely charged substrate by random sequential absorption (Adamczyk, Siwek, Zembala, & Belouschek, 1994). The repulsion within negatively charged polystyrene particles contributes to particle adsorption with similar short range distance between them. A Ti film of 20 nm was then evaporated by physical vapour deposition (PVD) to generate the hole-mask. Prior to 2 nm Ti and 20 nm Au evaporation by PVD, PS particles were removed and the exposed PMMA was etched away by Reactive-ion etching (RIE). The last step was the mask lift-off with acetone to create Au disks. Au disks were always cleaned prior to the sensing experiments. The molecular imprinted polymer was developed based on surface imprinting, in the same approach as for QCM-D and SPR experiments. Salivary proteins were covalently immobilized on the surface through amine coupling, followed by electrostatic interaction with the charged monomers and thiol monomer individually. The next step involved the molecular imprinting polymerization under mild conditions. Enzymatic protein digestion by proteinase k was used to remove the salivary proteins from the imprinting sites. The imprinting steps on Au disks were controlled by optical extinction spectroscopy. In parallel, and by excluding the salivary protein immobilization step, non-imprinted materials (NIP) were produced for control purposes. The imprinted materials (MIPs) and NIPs were used for salivary proteins rebinding followed by PGG interaction.

The fabricated Au disks showed a LSPR peak position of 697 ± 3 nm, before any chemical modification and in PBS pH 7. The small variation in the initial peak position for different sensor surfaces did not represent a problem for sensing because it is in the same spectral region and the detection would be based on peak shifts rather than peak positions. The subsequent modification steps of the Au disks were followed by LSPR, and can be seen in Fig. 3A. The covalent attachment of salivary proteins onto Au nanodisks induced an average peak shift of 7.3 ± 1.1 nm, showing more effectiveness than physical adsorption of saliva. This result suggested that during physical adsorption proteins may undergo conformational changes, and one protein molecule might occupy a larger surface area than an unfolded protein. The high peak shifts of saliva proteins resulted from the refractive index increase close to the metal nanostructure providing a red shift of the plasmon peak. The formation of polymer around the nanostructures provided a blue shift of 1.4 ± 0.7 and a red shift of 3.5 ± 1.3 nm for MIP and NIP, respectively. The blue shift verified for the MIP might result from some protein loss during polymerization considering that NIP showed a red shift which is still inferior to the total shift obtained by the MIP. The enzymatic digestion of salivary proteins by proteinase k resulted in the blue shift for both materials whereas peak shift for NIP materials were negligible with

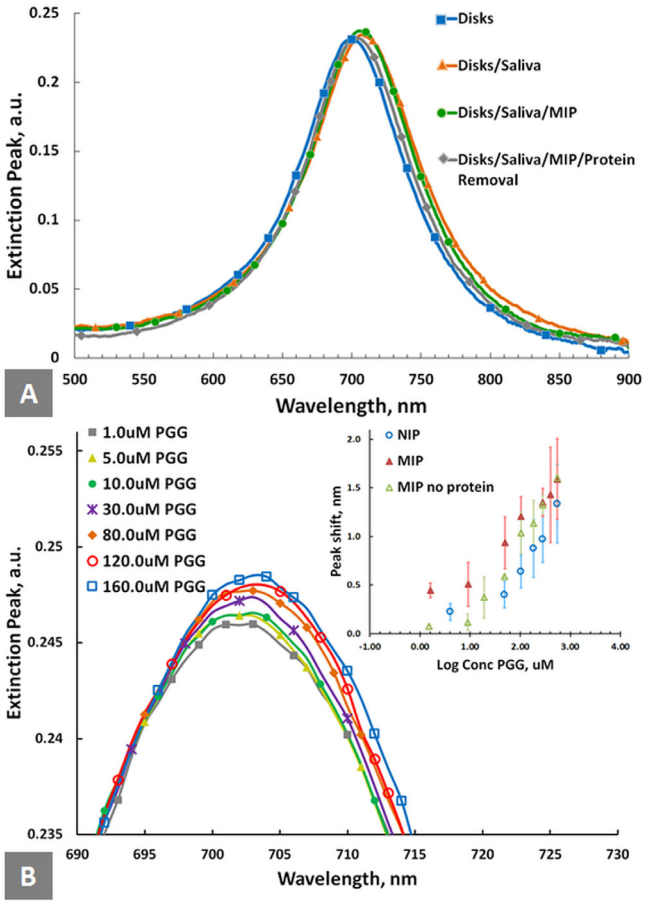

Fig. 3. (A) Molecular imprinting of saliva on Au nanodisks (ø 100 nm) followed by LSPR. Disks (Blue square), Disks/salivary protein (orange triangles), Disks/salivary proteins/Molecular imprinted polymer (green circles) and Disks/salivary proteins/Molecular imprinted polymer/Enzymatic proteins removal by proteinase k (purple diamonds). (B) LSPR calibration curve obtained for the interaction rebind salivary proteins and PGG, for the imprinting sensor materials with and without saliva rebinding. Inset: linear relation of peak shift *versus* log PGG concentration.

0.4 ± 0.02 compared to 2.8 ± 0.7 nm for MIP. These results were consistent with the QCM-D and SPR, showing efficient salivary proteins removal. At this stage both imprinted and non-imprinted materials were ready to be applied in the interaction studies.

The first rebinding was performed by incubating salivary proteins for ~20 min with the sensing surface in continuous flow. In this, the refractive index increased around the metal disks providing a red peak shift of 1.75 ± 0.76 and 0.75 ± 1.12 nm for MIP and NIP, respectively. The absolute peak shift for saliva digestion is slightly lower than the rebinding, indicating that for MIP ~65% binding sites were occupied by salivary proteins. Considering the NIP material, even though rebinding seems to some extent large, the rebinding is inconsistent resulting in unsystematic non-specific binding. The interaction with PGG was then carried out for 150 s in continuous flow followed by another 150 s of PBS 5% ethanol rinsing before taking the spectra. The interaction was established between salivary proteins and PGG solutions with increasing concentrations, ranging from 1.0 up to 140 μM. The response showed a linear red shift variation with the increasing concentrations. Fig. 3B displays the spectra shifts that corresponded to different PGG concentrations: the lowest PGG concentration corresponded to the grey curve and the highest concentration to the blue curve. The peak shift obtained for the lowest concentration was 0.39 ± 0.07 nm whereas for the highest concentration the peak shift achieved 2.00 ± 0.41 nm.

The stable red shift indicates that the binding of PGG to salivary proteins is strong with PGG remaining on the surface even after rinsing. The red shift for salivary proteins and for the highest PGG concentration is similar, but this does not mean that saliva and PGG bind with the same mass. The peak shift is based on the refractive index change around the metal nanodisks and PGG has a refractive index contribution around three times higher than salivary proteins. Thus, while the refractive index change of PGG interaction is larger than that generated by the protein layer formation, the amount of PGG should be lower.

For the controls, NIP and MIP without rebinding, the lower PGG concentration provided a peak shift of 0.25 ± 0.03 and 0.18 ± 0.08 nm while the highest PGG concentration was 1.60 ± 0.40 and 1.57 ± 0.03 nm, respectively. The controls had a similar behaviour, although the MIP with salivary proteins rebinding allowed obtaining higher and more stable responses. Indeed, the NIP response indicated that PGG interacted easily with the polymeric film used to imprint salivary proteins, a response that had no contribution to astringency. In turn, the rebinding of PGG to the MIP film was assumed to occur only on the protein layer, as the surface should be fully covered by saliva proteins. Thus, only the MIP response was directly linked to astringency, and the interaction between PGG and the control polymer is not relevant, assuming that the sensing surface was fully covered by proteins.

The results suggested that the interaction of complex protein matrix (saliva) with PGG could be assessed through the LSPR sensor, meaning that the system could be used to estimate wine astringency. For this, nine samples of 2012 red vinho verde from the Demarcated Region of Vinho Verde (Lima's sub-region) were used. Astringency estimation was carried out similarly to the interaction between saliva and PGG, however, in this case, PGG solutions were replaced by wine samples previously diluted 20-fold in PBS 5% ethanol.

The same samples were also analysed in terms of astringency through a sensorial panel (1–9 – lowest to the highest astringency level) in order to compare the two different methods. The peak shifts obtained by wine were used to calculate the PGG concentration and therefore estimate astringency expressed in PGG concentration. With no exception, all wines presented a red shift ranging from 0.12 to 0.97 nm, indicating that wine polyphenols were able to interact with the salivary proteins present on the LSPR sensor. The results in Table 2 showed the existence of a correlation between sensorial astringency and LSPR sensor astringency (with exception of wine G) and small deviations for most wines. The application of the LSPR sensor allowed the study of two complex matrices simultaneously, the saliva and red wine, showing good correlation with the sensorial panel.

Wine astringency estimation through a LSPR sensor was successfully applied in terms of PGG concentration. However there are many other compounds in the wines that may contribute to astringency, turning wine chemistry a crucial tool in this field. Thus, the wine samples were chemically characterized next, aiming to understand and support the previous data with other analytical tools.

3.4. Wine characterization

The wine samples were chemically characterized in terms of total phenolic content (TPC), proanthocyanic tannins, tannin power, dialysis index, free anthocyanins, monoglucosidic anthocyanins and in terms of colour (colour coordinates L^*, C^*, H^*; red colour index (RCI) and colour index (CI)). The samples were also tested for astringency sensorial analysis, performed externally (Comissão de Viticultura da Região dos Vinhos Verdes – CVRVV in Portugal) by an expert panel. Sensorial astringency was then compared with the analytical astringency measurements by LSPR sensor (LSPR astringency) and used as a reference.

To better understand the relationship between both astringency evaluation and the wine chemistry, principal component analysis (PCA) was performed on the full data set. PCA shows that sensor response for astringency and sensorial astringency are similar and also allowed to group wine samples into three subgroups.

First, PCA was applied to all the data of chemical and astringency evaluation. As shown in Fig. 4A biplot, the first component F1 accounts for 55.1% of variance and the second component, F2, for 19.9% (sum 75%). Generally, three main clusters of wine samples are revealed; one cluster (wine A and B) presents negative scores in PC1 while the other two clusters are positive. Within these two clusters, one contained four wine samples (wine C, D, G and F) with positive scores in PC2, and three wines with negative scores in PC2 (wine E, H and I). Regarding the variables, only two colour coordinates are presented in negative scores of PC1, while all the others are in the positive. This that wine samples A and B have the lower colour index and the higher lightness, meaning lower opacity and consequently lower colour intensity. For the PC2, LSPR astringency, monoglucosidic anthocyanins and tannin power are the dominant variables. For the cluster with wine samples C, D, G and F with positive scores in PC2 correspond to the samples with higher tannin power while the cluster with wine E, H and I have higher astringency levels. An interesting fact is that tannin power and LSPR/sensorial astringency are in opposite positions, indicating that polyphenols ability to precipitate proteins (in this case BSA) does not correlate well with astringency and therefore precipitation methods might lead to inaccurate astringency measurements (Mateus, Pinto, Ruao, & de Freitas, 2004). Moreover, both sensorial and LSPR astringency have similar positions in the biplot, showing that LSPR astringency can be used as an individual tool to estimate the parameter. Consistent with sensorial analysis, the wine samples classified as intermediate astringency levels are also positioned in slightly lower astringency intensity.

The wines that present higher reactivity toward BSA (tannin power), dialysis indexes, proanthocyanic tannins and total phenolic content were considered by the panel as medium astringency samples. Dialysis index is related to the complexity of tannins structure: the most complex structured tannins or highly charged molecules crossed the pores of a dialysis membrane at a slower rate than smaller molecules with lower charges. High dialysis

Table 2
LSPR response and astringency estimation expressed in PGG *versus* sensorial analysis for red wine samples.

Wine	Astringency intensity	Peak shift, nm	Astringency, expressed in PGG, μM	RSD%
A	1	0.33 ± 0.16	66 ± 2	4
B	2	0.57 ± 0.21	748 ± 95	13
C	3	1.10 ± 0.33	627 ± 93	15
D	4	0.67 ± 0.32	896 ± 72	8
E	6	0.93 ± 0.40	3585 ± 224	6
F	7	1.12 ± 0.63	13,326 ± 4159	31
G	8	1.19 ± 0.21	14,901 ± 5439	37
H	8	1.40 ± 0.66	15,019 ± 1183	8
I	9	1.49 ± 0.88	21,101 ± 8305	39

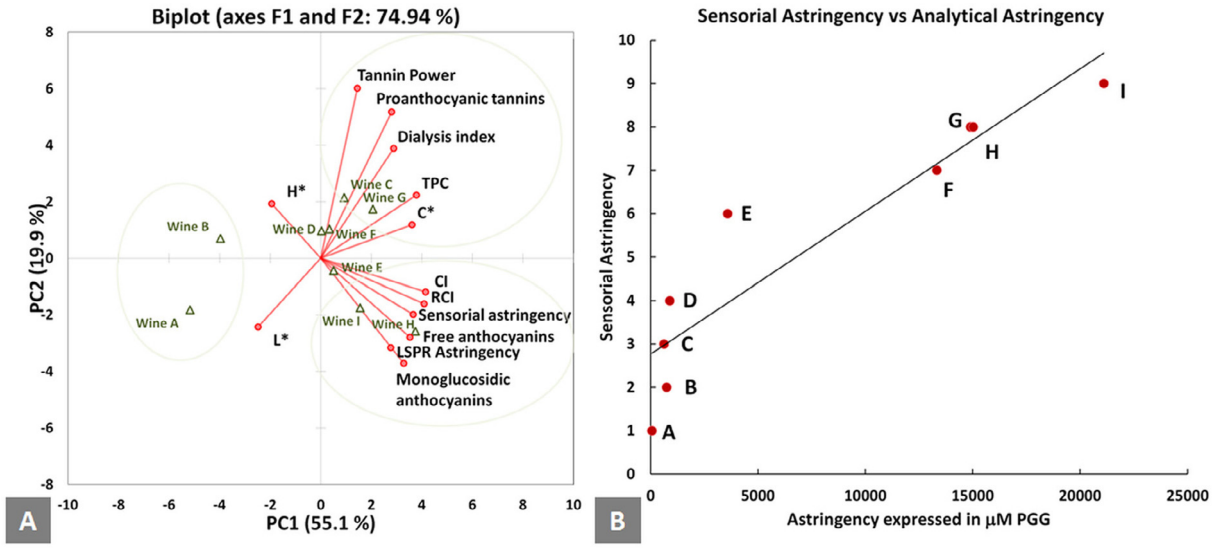

Fig. 4. (A) Biplot combined with loading plot from PCA of wine parameters. Each dot represents a wine sample and the vectors represent the parameters analysed. (B) Correlation between wine astringency, expressed in PGG *versus* sensorial panel analysis.

index indicated high structural complexity of wine compounds and in general, the ability of polyphenols to interact with proteins increases with polyphenols complexity. However, the precipitation ability of polyphenols is not a linear effect due to steric effect.

The wines with medium/high astringency sensorial analysis were also recently tested for prodelphinidin content (Teixeira, Azevedo, Mateus, & de Freitas, 2016). Several dimeric prodelphinidins were detected which can mean higher astringency. Vidal et al. refers that increased galloylation can be responsible for increased coarseness (rough texture, related to the feel of coarser grade emery paper) of the samples, whereas the trihydroxylation of the B-ring could decrease coarseness (Vidal et al., 2004). However, only medium astringency sensorial analysis wines were found to have trimeric prodelphinidins.

The biplot also indicated that samples with high astringency (sensorial and LSPR) correlated with high levels of colour index, red colour index, free anthocyanins and monoglucosidic anthocyanins. The red colour index might also be intensified by co-pigmentation events between anthocyanins and flavan-3-ol monomeric forms. Wine samples with high free anthocyanins content also showed high content for monoglucosidic anthocyanins indicating that these samples are likely to be young wines. Anthocyanins are the pigments responsible for wine red colour, thus high values for colour and red colour index are dependently correlated. Surprisingly, biplot suggests an intense relation between astringency, anthocyanins content and red colour. However, it is not yet clear to the scientific community the role played by anthocyanins in astringent perception (Soares, Brandão, Mateus, & Freitas, 2015), (Ferrer-Gallego et al., 2015). Even though the anthocyanins were considered non-astringent compounds, recent works have proved that anthocyanins can also interact effectively with salivary proteins (Ferrer-Gallego et al., 2015). Anthocyanins with great effect in red wine colour, were also pointed out as contributors for wine taste such as bitterness (Soares et al., 2013) and astringency. However, more work must be done in order to better clarify these sensorial properties of anthocyanins.

Therefore, the developed LSPR sensor seemed to be a useful tool to assess astringency by distinguishing and ranking the wine samples in terms of astringency levels, independently of the polyphenol content analysis.

The biplot showed that both sensorial astringency and LSPR astringency presented similar results, therefore a direct correlation of these two measurements was evidenced. Fig. 4B shows the relation between wine astringency expressed in PGG *versus* the sensory panel astringency, thus indicating the close agreement between both methodologies, as previously shown by the biplot. The linear correlation between these followed the equation.

$$\text{Astringency}_{\text{sensorial}} = 0.0003 \times \text{Astringency}_{\text{LSPR}} + 2.8 \text{ with a correlation coefficient of } 0.85$$

4. Conclusion

Here we applied a plasmonic/molecularly imprinted technology to study the molecular interactions of polyphenol compounds and saliva as the complex protein matrix to estimate astringency. We have quantified the saliva layer attached to the surface by QCM-

D and SPR techniques, to optimize the imprinting step of saliva. LSPR combined with surface imprinted polymers were then used to monitor polyphenol interactions with salivary protein and further astringency estimation, when applied to a range of real wine samples.

Astringency estimation was successfully applied to wine samples giving a response that was independent from individual chemical characterization. The LSPR astringency and sensorial analysis obtained from a trained sensorial panel correlated well, allowing the proposal of this method as a quantitative approach for real and practical application during wine production.

Acknowledgment

The authors acknowledge FCT, Fundação para a Ciência e Tecnologia, for the financial support (SFRH/BD/72479/2010), the European Social Fund, Fundo Social Europeu for the co-financial support. CVRVV (Comissão de Viticultura da Região dos VInhos verdes) is acknowledged for kindly providing the samples and their sensorial classification.

Appendix A. Supplementary data

Supplementary data associated with this article can be found, in the online version, at http://dx.doi.org/10.1016/j.foodchem.2017.04.051.

References

Adamczyk, Z., Siwek, B., Zembala, M., & Belouschek, P. (1994). Kinetics of localized adsorption of colloid particles. *Advances in Colloid and Interface Science, 48*, 151–280.

Batesmit, E. C. (1973). Hemanalysis of tannins – Concept of relative astringency. *Phytochemistry, 12*(4), 907–912.

Brand, H. S., Fat, G. M., & Veerman, E. C. I. (2009). The effects of saliva on the erosive potential of three different wines. *Australian Dental Journal, 54*(3), 228–232.

Caceres-Mella, A., Pena-Neira, A., Narvaez-Bastias, J., Jara-Campos, C., Lopez-Solis, R., & Canals, J. M. (2013). Comparison of analytical methods for measuring proanthocyanidins in wines and their relationship with perceived astringency. *International Journal of Food Science and Technology, 48*(12), 2588–2594.

Careri, M., Corradini, C., Elviri, L., Nicoletti, I., & Zagnoni, I. (2004). Liquid chromatography-electrospray tandem mass spectrometry of cis-resveratrol and trans-resveratrol: Development, validation, and application of the method to red wine, grape, and winemaking byproducts. *Journal of Agricultural and Food Chemistry, 52*(23), 6868–6874.

Chen, Y. M., & Hagerman, A. E. (2004). Characterization of soluble non-covalent complexes between bovine serum albumin and beta-1,2,3,4,6-penta-O-galloyl-D-glucopyranose by MALDI-TOF MS. *Journal of Agricultural and Food Chemistry, 52*(12), 4008–4011.

Dodds, M. W. J., Johnson, D. A., & Yeh, C. K. (2005). Health benefits of saliva: a review. *Journal of Dentistry, 33*(3), 223–233.

Ferrer-Gallego, R., Soares, S., Mateus, N., Rivas-Gonzalo, J., Escribano-Bailon, M. T., & de Freitas, V. (2015). New anthocyanin-human salivary protein complexes. *Langmuir, 31*(30), 8392–8401.

Fia, G., Dinnella, C., Bertuccioli, M., & Monteleone, E. (2009). Prediction of grape polyphenol astringency by means of a fluorimetric micro-plate assay. *Food Chemistry, 113*(1), 325–330.

Fredriksson, H., Alaverdyan, Y., Dmitriev, A., Langhammer, C., Sutherland, D. S., Zaech, M., & Kasemo, B. (2007). Hole-mask colloidal lithography. *Advanced Materials, 19*(23), 4297.

Freitas, V. A. P. D. (1995). *Recherches sur les tanins condensés: application à l'étude des structures et proprietés des procyanidines du raisin et du vin*. Bourdeaux: Université de Bourdeaux.

Furlan, A. L., Jobin, M.-L., Pianet, I., Dufburc, E. J., & Gean, J. (2015). Flavanol/lipid interaction: A novel molecular perspective in the description of wine astringency & bitterness and antioxidant action. *Tetrahedron, 71*(20), 3143–3147.

Glories, Y. (1978). *Recherches sur la matière colorante des vins rouges*. Bordeaux: Université de Bordeaux II.

Guerreiro, J. R. L., Bochenkov, V. E., Runager, K., Aslan, H., Dong, M. D., Enghild, J. J., ... Sutherland, D. S. (2016). Molecular imprinting of complex matrices at localized surface plasmon resonance biosensors for screening of global interactions of polyphenols and proteins. *ACS Sensors, 1*(3), 258–264.

Guerreiro, J. R. L., Frederiksen, M., Bochenkov, V. E., De Freitas, V., Ferreira Sales, M. G., & Sutherland, D. S. (2014). Multifunctional biosensor based on localized surface plasmon resonance for monitoring small molecule-protein interaction. *ACS Nano, 8*(8), 7958–7967.

Guerreiro, J. R. L., Sutherland, D. S., De Freitas, V., & Sales, M. G. F. (2013). Protein-polyphenol interaction on silica beads for astringency tests based on eye, photography or reflectance detection modes. *Analytical Methods, 5*(11), 2694–2703.

Hagerman, A. E., & Robbins, C. T. (1987). Implications of soluble tannin-protein complexes for tannin analysis and plant defense-mechanisms. *Journal of Chemical Ecology, 13*(5), 1243–1259.

He, F., Liang, N.-N., Mu, L., Pan, Q.-H., Wang, J., Reeves, M. J., & Duan, C.-Q. (2012). Anthocyanins and their variation in red wines II. Anthocyanin derived pigments and their color evolution. *Molecules, 17*(2), 1483–1519.

Hook, F., Voros, J., Rodahl, M., Kurrat, R., Boni, P., Ramsden, J. J., ... Kasemo, B. (2002). A comparative study of protein adsorption on titanium oxide surfaces using in situ ellipsometry, optical waveguide lightmode spectroscopy, and quartz crystal microbalance/dissipation. *Colloids and Surfaces B: Biointerfaces, 24*(2), 155–170.

Kawamoto, H., Nakatsubo, F., & Murakami, K. (1995). Quantitative-determination of tannin and protein in the precipitates by high-performance liquid-chromatography. *Phytochemistry, 40*(5), 1503–1505.

Kern, W., & Puotinen, D. A. (1970). Cleaning solutions based on hydrogen peroxide for use in silicon semiconductor technology. *RCA Review, 31*(2). 187.

Malmstrom, J., Agheli, H., Kingshott, P., & Sutherland, D. S. (2007). Viscoelastic Modeling of highly hydrated laminin layers at homogeneous and nanostructured surfaces: Quantification of protein layer properties using QCM-D and SPR. *Langmuir, 23*(19), 9760–9768.

Mateus, N., Pinto, R., Ruao, P., & de Freitas, V. (2004). Influence of the addition of grape seed procyanidins to Port wines in the resulting reactivity with human salivary proteins. *Food Chemistry, 84*(2), 195–200.

Mateus, N., Proenca, S., Ribeiro, P., Machado, J. M., & Freitas, V. d. (2001). Grape and wine polyphenolic composition of red Vitisvinifera varieties concerning vineyard altitude. *Ciencia y Tecnologia Alimentaria, 3*(2), 102–110.

Monteleone, E., Condelli, N., Dinnella, C., & Bertuccioli, M. (2004). Prediction of perceived astringency induced by phenolic compounds. *Food Quality and Preference, 15*(7–8), 761–769.

Obreque-Slier, E., Lopez-Solis, R., Pena-Neira, A., & Zamora-Marin, F. (2010). Tannin-protein interaction is more closely associated with astringency than tannin-protein precipitation: Experience with two oenological tannins and a gelatin. *International Journal of Food Science and Technology, 45*(12), 2629–2636.

Pascal, C., Poncet-Legrand, C., Cabane, B., & Vernhet, A. (2008). Aggregation of a proline-rich protein induced by epigallocatechin gallate and condensed tannins: Effect of protein glycosylation. *Journal of Agricultural and Food Chemistry, 56*(15), 6724–6732.

Ribéreau-Gayon, P., & Stonestreet, E. (1966). Le dosage des tanins dans le vin rouge et détermination de leur structure. *Chim. Anal., 48*, 188–192.

Rinaldi, A., Gambuti, A., & Moio, L. (2012). Application of the SPI (Saliva Precipitation Index) to the evaluation of red wine astringency. *Food Chemistry, 135*(4), 2498–2504.

Roggero, J. P., Larice, J. L., Rocheville-Divorne, C., Archier, P., & Coen, S. (1988). Compositionanthocyaniquedescépages. I. Essaideclassificationparanalyse encomposantesprincipalesetparanalysefactoriellediscriminante. (Anthocyanin composition of grape varieties. I. Classification attempt by using principal component analysis and discriminant factorial analysis.). *Revue Francaise d'Oenologie, 112*, 41–48.

Sarneckis, C. J., Dambergs, R. G., Jones, P., Mercurio, M., Herderich, M. J., & Smith, P. A. (2006). Quantification of condensed tannins by precipitation with methyl cellulose: Development and validation of an optimised tool for grape and wine analysis. *Australian Journal of Grape and Wine Research, 12*(1), 39–49.

Simoes Costa, A. M., Costa Sobral, M. M., Delgadillo, I., Cerdeira, A., & Rudnitskaya, A. (2015). Astringency quantification in wine: Comparison of the electronic tongue and FT-MIR spectroscopy. *Sensors and Actuators B-Chemical, 207*, 1095–1103.

Soares, S., Brandão, E., Mateus, N., & Freitas, V. D. (2015). Sensorial properties of red wine polyphenols: Astringency and bitterness. *Critical Reviews in Food Science and Nutrition*.

Soares, S., Kohl, S., Thalmann, S., Mateus, N., Meyerhof, W., & De Freitas, V. (2013). Different phenolic compounds activate distinct human bitter taste receptors. *Journal of Agricultural and Food Chemistry, 61*(7), 1525–1533.

Somers, T. C., & Evans, M. E. (1977). Spectral evaluation of young red wines – anthocyanin equilibria, total phenolics, free and molecular SO_2, chemical age. *Journal of the Science of Food and Agriculture, 28*(3), 279–287.

Somers, T. C., & Ziemelis, G. (1985). Spectral evaluation of total phenolic components in vitis-vinifera – grapes and wines. *Journal of the Science of Food and Agriculture, 36*(12), 1275–1284.

Teixeira, N., Azevedo, J., Mateus, N., & de Freitas, V. (2016). Proanthocyanidin screening by LC-ESI-MS of Portuguese red wines made with teinturier grapes. *Food Chemistry, 190*, 300–307.

Vidal, S., Courcoux, P., Francis, L., Kwiatkowski, M., Gawel, R., Williams, P., ... Cheynier, V. (2004). Use of an experimental design approach for evaluation of key wine components on mouth-feel perception. *Food Quality and Preference, 15*(3), 209–217.

Warkentin, P., Walivaara, B., Lundstrom, I., & Tengvall, P. (1994). Differential surface binding of albumin, immunoglobulin-G and fibrinogen. *Biomaterials, 15*(10), 786–795.

Whitcombe, M. J., Chianella, I., Larcombe, L., Piletsky, S. A., Noble, J., Porter, R., & Horgan, A. (2011). The rational development of molecularly imprinted polymer-based sensors for protein detection. *Chemical Society Reviews, 40*(3), 1547–1571.